Diagn Interv Radiol 2023; DOI: 10.4274/dir.2023.221849

HEAD AND NECK IMAGING

ORIGINAL ARTICLE

Comparison of image quality and quantitative parameters in intravoxel incoherent motion imaging at 3-T based on turbo spin-echo and echo-planar imaging in patients with oral cancer

Lingjie Yang#
Xing Wu#
Yu Wang
Guangzi Shi
Huijun Hu*
Xiaohui Duan*

#Lingjie Yang and Xing Wu contributed equally to this work.

***Xiaohui Duan and Huijun Hu are co-corresponding authors and equally contributed to this study.**

PURPOSE

To compare the image quality, apparent diffusion coefficient (ADC), and intravoxel incoherent motion- (IVIM) derived parameters of IVIM imaging based on turbo spin-echo (TSE) and echo-planar imaging (EPI) of patients with oral cancer and to assess the equivalence of the ADC and IVIM-derived parameters.

METHODS

Thirty patients with oral cancer underwent TSE-IVIM and EPI-IVIM imaging using a 3.0-T system. The distortion ratio (DR), signal-to-noise ratio (SNR), contrast-to-noise ratio (CNR), qualitative evaluations of image quality, ADC, pure diffusion coefficient (D), pseudo-diffusion coefficient (D*), and perfusion fraction (*f*) were compared between the two sequences. The consistency of the quantitative parameters in oral cancer between the TSE and EPI sequences was evaluated using a Bland–Altman analysis.

RESULTS

TSE-IVIM had a significantly smaller DR than EPI-IVIM ($P < 0.001$). The CNR of EPI-IVIM on most of the anatomical sites was significantly higher than that of TSE-IVIM ($P < 0.05$), while the SNR was not significantly different ($P > 0.05$). TSE-IVIM had significantly higher image quality, less distortion and artifacts, and lower image contrast compared with EPI-IVIM ($P < 0.05$). The lesion-edge sharpness and diagnostic confidence of EPI-IVIM were lower than that of TSE-IVIM, although no significant differences existed ($P > 0.05$). The ADC and D of TSE-IVIM had better reproducibility (intraclass correlation coefficient > 0.9). Although no significant difference existed for the ADC and IVIM-derived parameters of lesions between the two sequences ($P > 0.05$), wide limits of agreement were found in the Bland–Altman plots.

CONCLUSION

TSE-IVIM could be used as an alternative technique to EPI-IVIM for patients with oral cancer because of its better image quality. Furthermore, TSE-IVIM can provide more accurate quantitative parameters. However, the quantitative parameters derived from the two IVIM techniques cannot be used as equivalent parameters for patients with oral cancer.

KEYWORDS

Echo-planar imaging, image quality, intravoxel incoherent motion imaging, magnetic resonance imaging, oral cancer, quantitative parameters, turbo spin-echo

From the Department of Radiology (L.Y., X.W., Y.W., G.S., H.H. ✉ huhuijun@mail.sysu.edu.cn, X.D. ✉ duanxh5@mail.sysu.edu.cn), Sun Yat-Sen University, Sun Yat-Sen Memorial Hospital, Guangzhou, China; Guangdong Provincial Key Laboratory of Malignant Tumor Epigenetics and Gene Regulation (G.S., X.D.), Sun Yat-Sen Memorial Hospital, Sun Yat-Sen University, Medical Research Center, Guangzhou, China.

Received 01 September 2022; revision requested 29 November 2022; last revision received 25 January 2023; accepted 01 February 2023.

Epub: 20.03.2023

Publication date: 07.11.2023

DOI: 10.4274/dir.2023.221849

Oral cancer has become the 16th most common malignancy worldwide, occurring commonly in men of middle or old age in developing countries, with squamous cell carcinomas accounting for more than 90% of cases.[1-3] Diffusion-weighted imaging (DWI) with apparent diffusion coefficient (ADC), which can estimate the diffusion movement of water molecules and reflect the cellular density in tissues,[4-6] has been widely and routinely used in patients with oral cancer.[7,8] However, there is often a failure to distinguish the diffu-

You may cite this article as: Yang L, Wu X, Wang Y, Shi G, Hu H, Duan X. Comparison of image quality and quantitative parameters in intravoxel incoherent motion imaging at 3-T based on turbo spin-echo and echo-planar imaging in patients with oral cancer. *Diagn Interv Radiol.* 2023;29(6):786-793.

sion of water molecules from the perfusion of capillary blood when using ADC.[9] Multiple *b*-value-based intravoxel incoherent motion (IVIM) is an advanced DWI technique with the parameters of perfusion fraction (*f*), pure diffusion coefficient (D), and pseudo-diffusion coefficient (D*), which can avoid perfusion contamination and evaluate molecular diffusion and blood perfusion effects separately.[10,11] Therefore, IVIM imaging is being increasingly used for tumor detection, diagnosis, differential diagnosis, and prognostic evaluation for oral cancer.[12]

At present, single-shot echo-planar imaging (SS-EPI) is commonly applied for IVIM sequences, with the advantages of a rapid image acquisition speed and a relative insensitivity to motion.[13] Nevertheless, because of the complex structure of many air–bone boundaries and the presence of metallic dental implants in the head and neck, signal loss and geometric distortion are commonly found with SS-EPI due to the susceptibility artifacts and chemical shift artifacts in the phase-encoding direction,[14,15] which may result in a deterioration of image quality and a reduction in the diagnostic confidence of oral lesions. Alternatively, the single-shot turbo spin-echo (SS-TSE) uses multiple radiofrequency (RF) refocusing pulses, resulting in less susceptibility to artifacts and geometric distortions.[16] However, it commonly has the disadvantages of a lower signal-to-noise ratio (SNR) and a longer acquisition time.[17]

Recently, TSE-DWI sequences in 3-T magnetic resonance imaging (MRI) can shorten the scan time and obtain a higher SNR and less blurring through the reduction of echo space with the adoption of an appropriate RF pulse shape.[18] Some studies have reported that TSE-DWI had better image quality than EPI-DWI in breast cancer,[17] pulmonary lesions,[19] and orofacial lesions.[14,20] In addition, a preliminary study compared the image quality and the quantitative parameters derived from IVIM between the two IVIM sequences in a group of healthy volunteers' head and neck regions.[21] However, to our knowledge, comprehensive evaluation (including quantitative and qualitative) of image quality and comparisons of ADC, D, D*, and *f* between TSE-IVIM and EPI-IVIM in both oral lesions and normal anatomies of the head and neck have not been reported.

Thus, in this study, we evaluated and compared the geometric distortion, SNR, contrast-to-noise ratio (CNR), image quality, and ADC and IVIM-derived parameters in normal anatomies and oral lesions of TSE-IVIM and EPI-IVIM. The purpose of this study was to demonstrate whether TSE-IVIM can become an alternative technique to EPI-IVIM for patients with oral cancer and to determine the equivalence of these quantitative parameters.

Main points

- Turbo spin-echo (TSE)- intravoxel incoherent motion (IVIM) had better image quality in the oral and maxillofacial regions and could be used as an alternative technique to echo-planar imaging (EPI)-IVIM for patients with oral cancer.
- TSE-IVIM can provide more accurate parameter values, especially for the apparent diffusion coefficient and D values.
- The quantitative parameters acquired from TSE-IVIM and EPI-IVIM imaging cannot be used as equivalent parameters for the diagnosis and follow-up of oral cancer.

Methods

Patients

The Ethics Committee of Sun Yat-Sen Memorial Hospital, Sun Yat-Sen University (SYSEC-KY-KS-2022-029; 2022.01.19) approved this prospective study, and signed informed consent was given by all subjects. Patients with oral cancer requiring MR examination of the head and neck region prior to operation between May 2021 and December 2021 were included in our study. The exclusion criteria were as follows: (1) patients who had undergone a lesion biopsy before MRI; (2) patients who had a resection of the parotid gland, submandibular gland, or tongue; (3) patients who had contraindications for MR examinations that would affect the examination; or (4) patients in the early stage of pregnancy (less than 3 months). Finally, 30 patients, 19 (63.33%) males and 11 (36.67%) females, were included in this study. The mean age was 54 ± 10 years. Among them were 18 (60.00%) tongue carcinomas, 3 (10.00%) oral floor carcinomas, 3 (10.00%) gingiva carcinomas, 2 (6.67%) buccal carcinomas, 2 (6.67%) palate carcinomas, 1 (3.33%) oropharyngeal carcinoma, and 1 (3.33%) tonsil carcinoma.

Imaging protocol

All patients underwent MR examination using a 3-T MR system (Ingenia Digital Network Architecture 3.0 T, Philips Healthcare, Best, the Netherlands) with a 20-channel head and neck coil. SS-TSE- and SS-EPI-based IVIM sequences were executed consecutively in each examination. We used the same scanning parameters for the two IVIM sequences as far as it was feasible. In addition, 12 b values of 0, 20, 30, 50, 80, 100, 200, 500; 1,000; 1,500; 2,000, and 2,500 s/mm^2 were applied to the two IVIM sequences. The phase-encoding direction of both sequences was horizontal [left–right (LR)]. The scanning parameters of the two IVIM sequences and T2WI are shown in Table 1.

Data analysis

Image quality

Two experienced radiologists (S.G.Z. and D.X.H., with 6 and 10 years' experience in head and neck radiology, respectively), who were blinded to the scanning sequences and clinical information, independently performed quantitative and qualitative evaluations of the images' quality. The axial images of TSE-IVIM and EPI-IVIM with b = 1,000 s/mm^2 were selected and analyzed.

For the quantitative evaluation of image distortion, we calculated the distortion ratio (DR) at the level of the oral floor on the axial images of two IVIM images in comparison with that of axial TSE-T2WI images. We selected a representative slice level of the oral floor and displayed the TSE-IVIM, EPI-IVIM, and TSE-T2WI images on the same layer. Then, the LR width and anterior–posterior (AP) length of the whole image on transverse sections were measured on these three sequences. The DR was defined as the following equation:

$$DR = \frac{|A-B|}{B} \times 100\% , \quad (1)$$

where A is the anteroposterior or transverse diameter of the IVIM image and B is the anteroposterior or transverse diameter of the TSE-T2WI image. The DRs in both the LR and AP direction were calculated respectively.

The SNR and CNR were calculated for several normal anatomies and lesions on two kinds of IVIM images. The circular regions of interest (ROI) were placed in the bilateral parotid glands, bilateral submandibular glands, soft palate, tongue, oral floor, buccal mucosa soft tissue, lesion, and the muscles close to each organ, and the size of the ROIs was about 50 pixels. The mean and standard deviation (SD) of the signal intensity (SI) in each ROI were recorded. All ROIs of normal anatomical sites were delineated to avoid blood vessels, gland ducts, and lesions. For the measurements of CNR, adjacent muscles were used as the reference tissue. The SNR and CNR of each ROI were calculated as the following equations:

$$SNR = SI_a/SD_a\ , \quad (2)$$

$$CNR = |SI_a - SI_{muscle}|/SD_{muscle}\ , \quad (3)$$

where SI_a and SD_a represent the mean and SD of the SI in the normal anatomies or lesions, and SI_{muscle} and SD_{muscle} represent the mean and SD of the SI in the adjacent muscles.[20,21]

A 5-point scale was applied to qualitatively assess image quality, including image distortion, lesion-edge sharpness, image contrast, artifacts, overall image quality, and diagnostic confidence. Image distortion was recorded as follows: 1 = severe; 2 = obvious; 3 = moderate; 4 = slight; and 5 = no image distortion. Lesion-edge sharpness and image contrast for a normal anatomy were evaluated as follows: 1= unreadable; 2 = doubtful; 3 = moderate; 4 = good; and 5 = obvious. Chemical shift artifacts and susceptibility artifacts were evaluated, respectively, as follows: 1 = artifacts occur in the lesion and affect diagnosis; 2 = artifacts occur in more than three regions but do not affect the diagnosis; 3 = artifacts occur in three regions and do not affect the diagnosis; 4 = artifacts occur in less than three regions and do not affect the diagnosis; and 5 = almost no artifacts. Diagnostic confidence and overall image quality were scored as follows: 1 = not diagnostic; 2 = poor; 3 = moderate; 4 = good; and 5 = excellent.

ADC and quantitative parameters derived from IVIM

The ADC maps for this study were reconstructed using IntelliSpace Portal (version 9.0, Philips Healthcare), and the IVIM-derived parameter maps were generated by MITK-Diffusion (German Cancer Research Center, Germany).

Two radiologists delineated the ROIs in the bilateral parotid glands, bilateral submandibular glands, soft palate, tongue, oral floor, fat, muscle, and lesions on the ADC, D, D*, and *f* maps. The ROI of fat was set in the buccal area at the level of the tongue, and the sternocleidomastoid at the same level was designated as the ROI of the muscle. The ROIs were delineated to the maximum possible sizes to avoid blood vessels, gland ducts, and lesions. The ADC values were measured on each ADC parameter map by placing circular regions of multiple anatomical structures and lesions. A biexponential fit model was applied to calculate D, D*, and *f* according to a previous study.[21]

Statistical analysis

MedCalc (version 20.0, Mariakerke, Belgium) and SPSS (Version 25.0, IBM Corporation) software were used for all statistical analysis, with $P < 0.05$ representing statistical significance. Normally distributed data are expressed as mean ± SD, non-normally distributed data are displayed as median (minimum–maximum), and categorical variables are presented as frequencies with percentages. The qualitative evaluations and parameters of TSE-IVIM and EPI-IVIM were compared by using a paired Student's t-test and the Wilcoxon signed rank test. Interobserver agreement for continuous variables was estimated using the intraclass correlation coefficient (ICC). The levels of interobserver agreement were assessed as follows: 0–0.50 = poor, 0.51–0.75 = moderate, 0.76–0.90 = good, and 0.91–1.00 = excellent.[11] Additionally, the interobserver agreement of categorical variables was assessed using Kappa statistics: poor (0–0.20), fair (0.21–0.40), moderate (0.41–0.60), good (0.61–0.80), and excellent (0.81–1.00).[18] Furthermore, the consistency of the qualitative parameters of lesions between the two IVIM sequences was evaluated using a Bland–Altman analysis with 95% limits of agreement (LoA).

Table 1. The scanning parameters of T2WI, SS-TSE-IVIM, and SS-EPI-IVIM

	T2WI	SS-TSE-IVIM	SS-EPI-IVIM
TR/TE (ms)	2906/90	4488/89	5037/81
FOV (mm^2)	230 × 230	230 × 230	230 × 230
Matrix size	252 × 160	92 × 92	92 × 92
Voxel size (mm)	0.79 × 1.44	2.5 × 2.5	2.5 × 2.5
Reconstruction voxel size (mm)	0.53 × 0.53	0.96 × 0.96	0.8 × 0.8
SENSE factor	/	3.5	3.5
TSE/EPI factor	20 (TSE)	53 (TSE)	23 (EPI)
Slice thickness (mm)	5	5	5
Interlayer spacing (mm)	0.5	1	1
Flip angle	90°	90°	90°
Bandwidth (Hz/pixel)	698.6/0.6	652.7/0.7	68.0/6.4
NSA	2	2	2
Acquisition time	1 min 38 s	10 min 55 s	10 min 19 s

IVIM, intravoxel incoherent motion; SS-TSE, single-shot turbo spin echo; SS-EPI, SS echo-planar imaging; TR, repetition time; TE, echo time; FOV, field of view; NSA, number of signal averaged.

Results

Comparison of distortion ratio

The interobserver agreement of DRs was good ($P < 0.05$). The ICCs of DRs in the direction of LP and AP were 0.819 (TSE-IVIM) and 0.764 (EPI-IVIM), and 0.819 (TSE-IVIM) and 0.779 (EPI-IVIM), respectively. The mean DRs in the LR direction in TSE-IVIM and EPI-IVIM were 11.4% ± 5.1% and 15.1% ± 5.2%, and the mean DRs in the AP direction in TSE-IVIM and EPI-IVIM were 9.93% ± 2.65% and 11.8% ± 2.65%, respectively. Compared with EPI-IVIM, the DRs in both directions were significantly lower in TSE-IVIM ($P < 0.001$) (Figure 1), and the difference was more significant in the direction of LR, which was the phase-encoding direction.

Comparison of SNR and CNR

The SNR values showed good agreement between the two observers (ICC: 0.825 in TSE-IVIM and 0.829 in EPI-IVIM, $P < 0.05$), and the CNR values showed good to excellent agreement (ICC: 0.962 in TSE-IVIM and 0.873 in EPI-IVIM, $P < 0.05$). As shown in Table 2, no significant differences in SNR existed between the two IVIM sequences ($P > 0.05$) in the normal anatomical sites and the lesions. However, EPI-IVIM had significantly higher CNRs in the tongue, oral floor, buccal mucosa soft tissue, parotid glands, submandibular glands, and lesion compared with TSE-IVIM ($P < 0.05$), while no significant difference of the CNRs in the soft palate was found between the two IVIM techniques ($P = 0.417$).

Comparison of qualitative evaluations

Moderate to excellent interobserver agreements of the qualitative evaluations were obtained ($P < 0.05$). The Kappa values were 0.783 (TSE-IVIM) and 0.684 (EPI-IVIM) for image distortion, 0.896 (TSE-IVIM) and 0.906 (EPI-IVIM) for lesion-edge sharpness, 0.563 (TSE-IVIM) and 0.604 (EPI-IVIM) for image contrast, 0.851 (TSE-IVIM) and 0.819 (EPI-

IVIM) for diagnostic confidence, 0.873 (TSE-IVIM) and 0.907 (EPI-IVIM) for chemical shift artifacts, 0.750 (TSE-IVIM) and 0.634 (EPI-IVIM) for susceptibility artifacts, and 0.561 (TSE-IVIM) and 0.648 (EPI-IVIM) for overall image quality. The mean scores of the qualitative evaluations of image quality on TSE-IVIM and EPI-IVIM are shown in Figure 2. TSE-IVIM had significantly less image distortion, chemical shift artifacts, and susceptibility artifacts than EPI-IVIM ($P < 0.001$). The lesion-edge sharpness and diagnostic confidence of EPI-IVIM were lower than for TSE-IVIM, although no significant differences existed ($P > 0.05$). EPI-IVIM had significantly higher image contrast than TSE-IVIM ($P < 0.05$), although TSE-IVIM had significantly higher overall image quality than EPI-IVIM ($P < 0.001$). Representative IVIM images are presented in Figures 3, 4.

Comparison of ADC and quantitative parameters derived from IVIM

The ICCs of ADC and IVIM-derived parameters in the normal anatomical sites and lesions on TSE-IVIM and EPI-IVIM are shown in Table 3. Good to excellent interobserver agreement was found for ADC, and the interobserver agreement for TSE was similar to that for EPI. The interobserver agreement of D was moderate to excellent, and the interobserver agreement of TSE was better than that of EPI. The measurement consistency of D* and *f* was relatively poor. The interobserver agreement for D* was moderate to good, and no obvious difference existed between TSE and EPI. The interobserver agreement for *f* was moderate to excellent, and no obvious difference existed between TSE and EPI.

Table 3 summarizes the mean ADC, D, D*, and *f* values derived from the two IVIMs. No significant differences in the values of ADC, D, D*, and *f* were found in lesions and fat ($P > 0.05$). The ADC values of the right parotid gland, right submandibular gland, and oral floor were not significantly different between the two sequences ($P > 0.05$). The ADC values of the soft palate in EPI-IVIM were lower than those in TSE-IVIM ($P = 0.033$). In addition, EPI-IVIM had higher ADC values than TSE-IVIM in other parts ($P < 0.05$). The D values of the tongue and oral floor were not significantly different between the two sequences ($P > 0.05$). The D values of EPI-IVIM were higher than those of TSE-IVIM in other parts except the soft palate, which was lower in EPI-IVIM ($P < 0.05$). The D* values of the parotid glands, soft palate, and muscle in TSE-IVIM and EPI-IVIM were not significantly different ($P > 0.05$). However, in the other parts, D* of EPI-IVIM exhibited higher values than for TSE-IVIM ($P < 0.05$). The *f* values for the oral floor, submandibular glands, and parotid glands were not significantly different between the two sequences ($P > 0.05$). The *f* values of the soft palate and tongue were higher for TSE-IVIM than EPI-IVIM, while the *f* values of muscle were higher for EPI-IVIM ($P < 0.05$).

As shown in Figure 5, the Bland–Altman plots exhibit a consistency in the quantitative parameters for lesions between the two IVIM sequences. The 95% LoAs were −1.12 to 1.53 for ADC, −0.84 to 0.70 for D, −32.0 to 31.7 for D*, and −27.5 to 27.8 for *f*. No fixed biases between the two sequences were found regarding ADC ($P = 0.107$), D ($P = 0.341$), D* ($P = 0.949$), or *f* ($P = 0.952$) values for lesions. However, the 95% LoAs shown in the plots were wide between TSE-IVIM and EPI-IVIM.

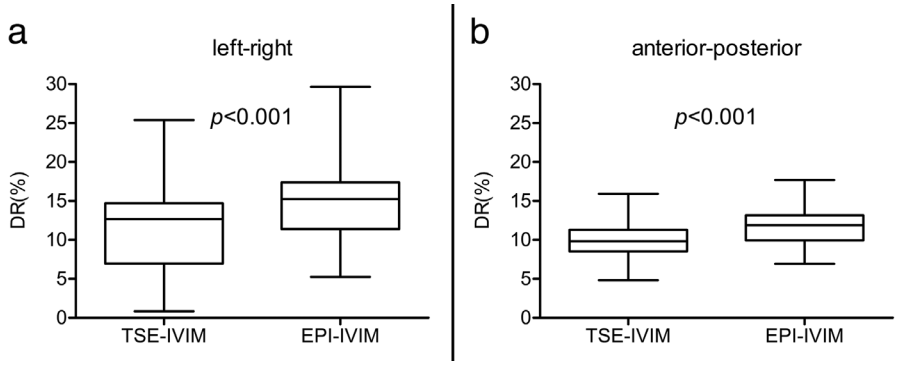

Figure 1. Box-and-whisker plots for the distortion ratios (DRs) of turbo spin-echo intravoxel incoherent motion (TSE-IVIM) and echo-planar imaging (EPI) IVIM. The DRs of the **(a)** left–right width and **(b)** anterior–posterior length were significantly lower in the images of TSE-IVIM than in those of EPI-IVIM ($P < 0.001$ by paired Student's t-test).

Discussion

Our results demonstrated that TSE-IVIM had significantly less image distortion, chemical-shift artifacts, and susceptibility artifacts than EPI-IVIM in patients with oral cancer. TSE-IVIM had better lesion-edge sharpness and higher diagnostic confidence than EPI-IVIM, although no statistical differences existed. SNR had no significant differences, while EPI-IVIM had significantly higher CNR on most anatomical structures and lesions in comparison with TSE-IVIM, indicating that EPI-IVIM had significantly higher image contrast than TSE-IVIM. On the whole, TSE-IVIM

Table 2. The SNR and CNR on TSE-IVIM and EPI-IVIM

	SNR (n = 30)			CNR (n = 30)		
	TSE-IVIM	EPI-IVIM	*P*	TSE-IVIM	EPI-IVIM	*P*
Parotid gland (L)	8.9 (5.3–19.9)	9.2 (6.2–24.7)	0.072	1.9 (0.3–7.2)	4.3 (0.2–20.2)	0.004
Parotid gland (R)	9.0 (4.4–16.0)	8.3 (3.8–18.7)	0.165	2.1 (0.1–11.1)	4.9 (0.3–35.6)	0.003
Submandibular gland (L)	9.1 (5.9–19.1)	8.0 (4.9–19.9)	0.309	4.4 (0.2–17.9)	7.0 (1.5–29.2)	<0.001
Submandibular gland (R)	9.8 (5.8–23.2)	9.4 (5.1–28.2)	0.673	3.4 (0.3–15.5)	6.4 (0.2–29.5)	<0.001
Soft palate	6.3 (4.0–12.7)	7.2 (3.0–12.7)	0.734	5.5 (1.5–12.3)	4.9 (0.5–14.8)	0.417
Tongue	7.7 (4.0–13.1)	7.8 (3.5–16.4)	0.098	3.1 (0.2–6.9)	5.0 (1.1–10.8)	0.002
Oral floor	8.2 (3.9–15.6)	6.7 (4.5–10.8)	0.185	1.2 (0.2–7.2)	3.9 (0.2–25.8)	<0.001
Buccal mucosa soft tissue	9.0 (3.5–12.7)	7.6 (3.9–12.5)	0.199	0.8 (0.2–15.5)	1.3 (0.1–19.8)	0.047
Lesion	10.6 (6.9–36.0)	10.8 (4.1–32.5)	0.517	13.1 (1.5–70.9)	16.2 (1.5–109.7)	0.037

Data are presented as median (minimum–maximum). IVIM, intravoxel incoherent motion; TSE, turbo spin echo; EPI, echo-planar imaging; SNR, signal-to-noise ratio; CNR, contrast-to-noise ratio.

had better overall image quality than EPI-IVIM. The ADC and D values showed good interobserver agreement, while the measurement consistency of D* and *f* was poor. Moreover, TSE-IVIM exhibited higher measurement consistency of ADC and D than EPI-IVIM. Additionally, although no fixed bias existed for the ADC, D, D*, and *f* values of lesions between the two sequences, the Bland–Altman plots showed wide 95% LoAs.

Clinically, SS-EPI is the most commonly used technique for IVIM sequences. However, artifacts and geometric distortions in EPI-IVIM are usually prominent in patients with oral cancer because of the presence of air–tissue interfaces or metallic implants in the oral and maxillofacial region, which may negatively impact on the reproducibility and reliability of IVIM and the derived quantitative parameters.[10] Theoretically, artifacts and geometric distortions in EPI sequences are prone to arise in the phase-encoding direction because of the acquisition of each echo at a different echo time and the accumulation of phase errors caused by rotating protons without RF refocusing pulses. In contrast, TSE sequences acquire multiple echoes at each excitation and apply RF refocusing pulses to reduce magnetic field inhomogeneity and avoid the accumulation of phase errors; hence, TSE sequences usually have less image distortion, chemical shift artifacts, and susceptibility artifacts than EPI sequences.[14,18] In our study, TSE-IVIM showed better image quality on account of lower levels of image distortion and artifacts than EPI-IVIM, which was in agreement with previous studies on the head and neck region[14,20,22] and the whole body.[23] The artifacts within and around the lesions in EPI-IVIM images could reduce the lesion-edge sharpness and diagnostic confidence for oral cancer. Therefore, the reduction of image distortion and artifacts using TSE-IVIM may facilitate a better diagnostic confidence for oral cancer.

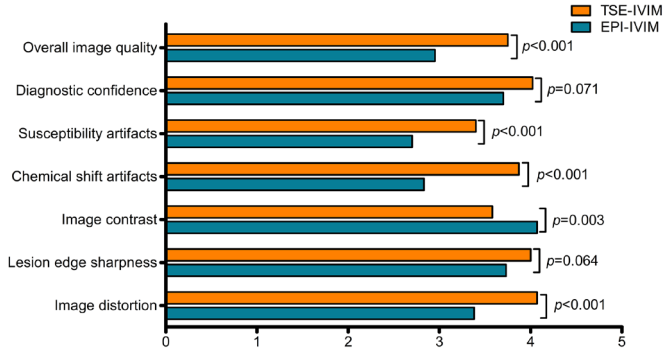

Figure 2. Bar chart showing the mean scores of qualitative evaluations of image quality for turbo spin-echo intravoxel incoherent motion (TSE-IVIM) and echo-planar imaging (EPI) IVIM images. The *P* values acquired using Wilcoxon's signed rank test are shown on the right side for comparison of the two sequences.

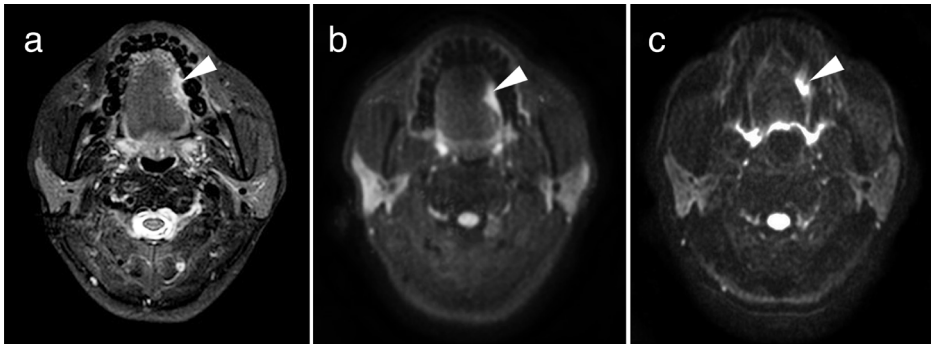

Figure 3. **(a)** T2WI fat-suppressed, **(b)** turbo spin-echo intravoxel incoherent motion (TSE-IVIM) b1000, and **(c)** echo-planar imaging (EPI) IVIM b1000 of a 58-year-old man with squamous cell carcinoma on the left tongue edge. The lesion on **(b)** TSE-IVIM b1000 is shown in accordance with **(a)** T2WI fat-suppressed. However, obvious geometric distortion of lesion (arrowheads) is seen on **(c)** EPI-IVIM b1000 compared with that on **(b)** TSE-IVIM b1000.

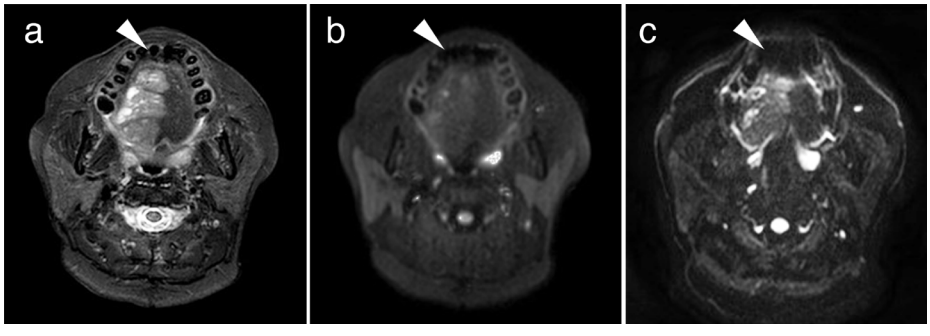

Figure 4. **(a)** T2WI fat-suppressed, **(b)** turbo spin-echo intravoxel incoherent motion (TSE-IVIM) b1000, and **(c)** echo-planar imaging (EPI) IVIM b1000 of a 54-year-old female with squamous cell carcinoma on the right half of the tongue. **(c)** EPI-IVIM b1000 has more susceptibility artifacts (arrowheads), which affect the display of some parts of the lesion, in comparison with **(b)** TSE-IVIM b1000. However, the lesion in **(c)** EPI-IVIM b1000 shows higher contrast than that in **(b)** TSE-IVIM b1000.

As for SNR and CNR, previous studies have shown that TSE-DWI had inherently lower SNR in comparison with EPI-DWI as a result of multiple RF refocusing pulses.[13,22,24] Nevertheless, some studies had opposite results, with significantly higher SNR and CNR occurring in TSE-DWI compared with in EPI-DWI.[20,21] Shorter RF pulses owing to the adjustment of RF pulse shape can contribute to higher SNR and less blurring in TSE-DWI. In the present study, IVIM and EPI-IVIM showed similar SNRs; this is different to the aforementioned studies but consistent with some reports that showed both sequences had comparable SNRs in the lung.[19,25] However, EPI-IVIM had higher CNR in comparison with TSE-IVIM in our study, which was oppositive to the reports in previous studies.[20,21] These differences might have resulted from the higher noise (SD value) of TSE-IVIM in comparison with that of EPI-IVIM in our study. Various parameters of image acquisition, including the voxel size, receiver bandwidth, and number of signal averaged (NSA), can affect image noise.[26,27] In our study, the voxel size and NSA of the two sequences were the same, while the TSE-IVIM sequence had an obviously wider bandwidth (932.4 Hz/pixel) than EPI-IVIM (10.6 Hz/pixel). The wider bandwidth in TSE-IVIM leads to greater image noise.[24] In contrast, the bandwidth of TSE-IVIM in previous studies was smaller than that seen in EPI-IVIM, thus inducing the lower noise of TSE-IVIM.[20,21] According to the formulae of SNR and CNR in our study, the higher SI and the higher level of noise in TSE-IVIM resulted in a similar SNR to that of EPI-IVIM, and the larger amount of noise of the adjacent muscles used as the reference tissue led to a lower CNR in TSE-IVIM.

Table 3. The ADC and IVIM-derived parameters and their ICCs on TSE-IVIM and EPI-IVIM

	ADC ($\times 10^{-3}$ mm^2/s) (n = 30)			D ($\times 10^{-3}$ mm^2/s) (n = 30)			D* ($\times 10^{-3}$ mm^2/s) (n = 30)			*f* (%) (n = 30)		
	TSE-IVIM (ICC)	EPI-IVIM (ICC)	*P*	TSE-IVIM (ICC)	EPI-IVIM (ICC)	*P*	TSE-IVIM (ICC)	EPI-IVIM (ICC)	*P*	TSE-IVIM (ICC)	EPI-IVIM (ICC)	*P*
Parotid gland (L)	1.38 ± 0.62 (0.990*)	1.56 ± 0.52 (0.991*)	0.017	0.30 ± 0.13 (0.943*)	0.45±0.11 (0.678*)	<0.001	44.02 ± 13.82 (0.840*)	40.74 ± 12.95 (0.721*)	0.262	22.49 ± 5.49 (0.751*)	24.22 ± 5.78 (0.621*)	0.318
Parotid gland (R)	1.36 ± 0.67 (0.994*)	1.78 ± 1.91 (0.995*)	0.441	0.28 ± 0.14 (0.938*)	0.33±0.14 (0.660*)	0.001	42.62 ± 15.94 (0.745*)	49.65 ± 18.80 (0.763*)	0.079	25.77 ± 7.84 (0.692*)	28.37 ± 6.65 (0.732*)	0.165
Submandibular gland (L)	1.74 ± 0.62 (0.994*)	2.01 ± 0.58 (0.987*)	0.001	0.41 ± 0.17 (0.947*)	0.60±0.26 (0.927*)	<0.001	31.76 ± 9.19 (0.835*)	36.87 ± 11.67 (0.732*)	0.047	34.25 ± 10.46 (0.736*)	30.91 ± 8.52 (0.812*)	0.052
Submandibular gland (R)	1.88 ± 0.67 (0.994*)	2.01 ± 0.56 (0.997*)	0.162	0.43 ± 0.14 (0.873*)	0.62±0.18 (0.891*)	<0.001	25.73 ± 8.14 (0.751*)	39.46 ± 16.20 (0.639*)	0.001	35.82 ± 8.16 (0.910*)	32.36 ± 10.57 (0.692*)	0.079
Soft palate	1.41 ± 0.50 (0.996*)	1.18 ± 0.48 (0.995*)	0.033	0.34 ± 0.12 (0.918*)	0.30±0.17 (0.927*)	0.016	56.77 ± 19.16 (0.826*)	57.45 ± 15.36 (0.566*)	0.959	29.31 ± 8.95 (0.730*)	26.04 ± 8.44 (0.771*)	0.032
Tongue	1.04 ± 0.54 (0.977*)	0.73 ± 0.52 (0.965*)	<0.001	0.19 ± 0.12 (0.843*)	0.16±0.13 (0.896*)	0.067	43.99 ± 15.82 (0.818*)	60.52 ± 19.05 (0.623*)	<0.001	29.67 ± 6.23 (0.751*)	24.40 ± 8.30 (0.548*)	0.002
Oral floor	0.92 ± 0.37 (0.992*)	1.02 ± 0.46 (0.993*)	0.178	0.14 ± 0.06 (0.936*)	0.20±0.16 (0.901*)	0.417	40.93 ± 13.74 (0.769*)	55.03 ± 19.09 (0.869*)	<0.001	29.81 ± 6.84 (0.650*)	27.94 ± 8.40 (0.859*)	0.159
Fat	0.19 ± 0.11 (0.978*)	0.18 ± 0.15 (0.976*)	0.168	0.06 ± 0.02 (0.844*)	0.08±0.05 (0.672*)	0.276	74.98 ± 11.54 (0.602*)	72.08 ± 17.79 (0.868*)	0.719	16.39 ± 5.05 (0.662*)	16.56 ± 7.45 (0.916*)	0.750
Muscle	0.39 ± 0.27 (0.922*)	0.84 ± 0.51 (0.892*)	<0.001	0.11 ± 0.08 (0.906*)	0.21±0.11 (0.772*)	<0.001	62.27 ± 17.68 (0.611*)	60.21 ± 15.90 (0.706*)	0.644	19.69 ± 6.65 (0.722*)	25.29 ± 5.80 (0.741*)	0.001
Lesion	2.37 ± 0.88 (0.983*)	2.16 ± 0.80 (0.977*)	0.086	0.66 ± 0.19 (0.916*)	0.73±0.35 (0.595*)	0.376	29.52 ± 14.09 (0.812*)	29.70 ± 13.83 (0.816*)	0.894	27.07 ± 11.17 (0.762*)	26.91 ± 10.36 (0.861*)	0.600

$P < 0.05$. Data are presented as mean ± standard deviation. ICC, intraclass correlation coefficient; IVIM, intravoxel incoherent motion; TSE, turbo spin echo; EPI, echo-planar imaging; ADC, apparent diffusion coefficients; D, pure diffusion coefficients; D, pseudo-diffusion coefficient; *f*, perfusion fraction.

In terms of the reproducibility of ADC, D, D*, and *f*, we found that the interobserver agreements for ADC and D were satisfactory, indicating that ADC and D were robust parameters in the head and neck region, while D* and *f* had relatively poor reproducibility and high observer variability based on the lower ICC in both the TSE and EPI sequences, which was in accordance with many previous studies.[28-31] Additionally, in our study, the ADC and D values of TSE-IVIM showed higher measurement consistency than those of EPI-IVIM, especially the D values. This result indicated that TSE-DWI had higher interobserver agreement of ADC and D in comparison to EPI-DWI, similar to some previous studies.[11,32] TSE-IVIM was prone to decreased measurement errors, which may be on account of fewer geometric distortions and susceptibility artifacts, thus impairing interobserver accordance for ADC and D.[11]

In addition, our results showed that the values of D, D*, *f*, and ADC derived from the two sequences were not completely identical. TSE-IVIM and EPI-IVIM had comparable D, D*, *f*, and ADC values only in lesions and fat. However, no significant differences of certain parameters in some normal anatomical structures existed between TSE-IVIM and EPI-IVIM, which was in line with a previous study.[21] Furthermore, based on the absence of significant differences for IVIM-derived parameters in lesions between TSE-IVIM and EPI-IVIM, a Bland–Altman analysis of TSE-IVIM and EPI-IVIM was performed in our study; it demonstrated that the parameters of lesions derived from TSE-IVIM and EPI-IVIM had no fixed bias, yet the 95% LoAs were wide, suggesting that the LoAs in lesions between the two sequences were unacceptable, similar to some previous results.[11,21] Wan et al.[11] reported that the 95% LoAs of ADC and D were up to 60% and 62%, respectively, between EPI and TSE in pulmonary neoplasms. Mikayama et al.[21] also found wide 95% LoAs for ADC, D, and *f* in the normal anatomy of the head and neck. A number of reasons may explain these differences and the wide 95% LoAs between TSE-IVIM and EPI-IVIM. First, the independent ROI delineation of both sequences might result in such differences. Although we attempted to draw the ROIs at the same level with the same size as much as possible, the two ROIs drawn for the two different sequences unavoidably had some differences in terms of size and exact position.[32] Second, geometric distortions caused by susceptibility artifacts observed within the tumor region in the EPI sequence will negatively impact the measurement precision of diffusion parameters.[32] Finally, these parameters can also be influenced by image noise, which may decrease with the increase of image noise.[18] Therefore, D, D*, *f*, and ADC derived from IVIM based on TSE and EPI cannot be regarded as equivalent parameters for the differential diagnosis and efficacy evaluation of oral cancer.

The present study has some limitations. First, the scanning parameters of the two sequences were not identical; for example, TSE-IVIM and EPI-IVIM used different receiver bandwidths. However, the two se-

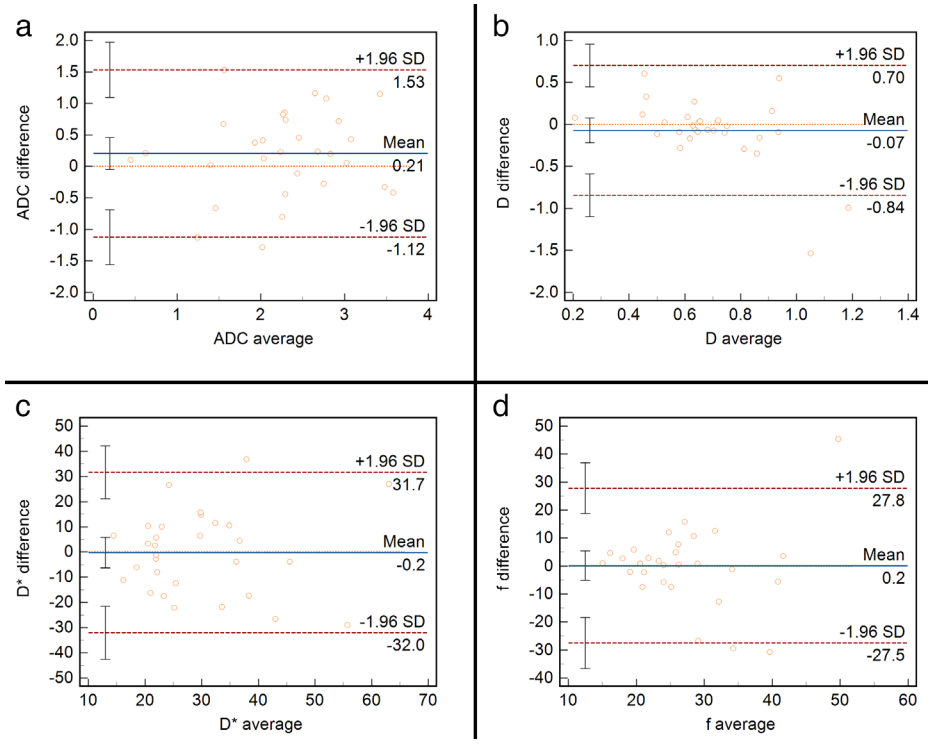

Figure 5. Bland–Altman plots for **(a)** apparent diffusion coefficient (ADC), **(b)** diffusion coefficient (D), **(c)** pseudo-diffusion coefficient (D*), and **(d)** perfusion fraction (*f*) of turbo spin-echo intravoxel incoherent motion (TSE-IVIM) and echo-planar imaging IVIM in the lesions. Continuous blue lines indicate mean differences, and dotted red lines indicate 95% limits of agreement (LoA). There were no fixed biases between the two sequences. However, the 95% LoAs were wide.

quences had similar scanning times in our study, although the scanning time for TSE-DWI is longer in clinical practice. Second, the acquisition time was relatively long in this study, lasting more than 10 minutes in both sequences. We used 12 *b* values in both IVIM sequences. In spite of the improvement in accuracy for IVIM-derived parameters using a large number of b values, it significantly prolonged the scanning time, resulting in more motion artifacts, and it is not clinically applicable for limited imaging time. Nevertheless, no obvious motion artifacts were detected for either TSE-IVIM or EPI-IVIM in this study. Third, the data we acquired with a 3-T system cannot be extrapolated to 1.5-T systems. On account of the difference in magnetic field strength, 1.5-T MRI scanners have less magnetic susceptibility artifacts and magnetic field inhomogeneity compared with 3-T scanners.[30] This indicates that the advantage of TSE-DWI having less susceptibility artifacts and geometric distortions may be less significant when used with 1.5-T systems. Accordingly, further research comparing MRI scanners with different magnetic field strengths is necessary.

In conclusion, TSE-IVIM in the oral and maxillofacial regions provides better image quality with less geometric distortion and fewer artifacts than EPI-IVIM. Thus, TSE-IVIM could be used as an alternative technique to EPI-IVIM in patients with oral cancer, especially in those with metallic implants prone to producing artifacts. Furthermore, ADC and D derived from TSE-IVIM have good reproducibility, indicating that TSE-IVIM can provide more accurate parameter values. However, the D, D*, *f*, and ADC values derived from IVIM based on the two sequences cannot be used as equivalent parameters for the diagnosis and follow-up of oral cancer.

Conflict of interest disclosure

The authors declared no conflicts of interest.

References

1. Montero PH, Patel SG. Cancer of the oral cavity. *Surg Oncol Clin N Am*. 2015;24(3):491-508. [CrossRef]
2. Warnakulasuriya S, Kerr AR. Oral cancer screening: past, present, and future. *J Dent Res*. 2021;100(12):1313-1320. [CrossRef]
3. D'souza S, Addepalli V. Preventive measures in oral cancer: an overview. *Biomed Pharmacother*. 2018;107:72-80. [CrossRef]
4. Connolly M, Srinivasan A. Diffusion-weighted imaging in head and neck cancer: technique, limitations, and applications. *Magn Reson Imaging Clin N Am*. 2018;26(1):121-133. [CrossRef]
5. Widmann G, Henninger B, Kremser C, Jaschke W. MRI sequences in head & neck radiology - state of the art. *Rofo*. 2017;189(5):413-422. [CrossRef]
6. Iima M, Yamamoto A, Kataoka M, et al. Time-dependent diffusion MRI to distinguish malignant from benign head and neck tumors. *J Magn Reson Imaging*. 2019;50(1):88-95. [CrossRef]
7. Koontz NA, Wiggins RH. Differentiation of benign and malignant head and neck lesions with diffusion tensor imaging and DWI. *AJR Am J Roentgenol*. 2017;208(5):1110-1115. [CrossRef]
8. Norris CD, Quick SE, Parker JG, Koontz NA. Diffusion MR imaging in the head and neck: principles and applications. *Neuroimaging Clin N Am*. 2020;30(3):261-282. [CrossRef]
9. Payabvash S. Quantitative diffusion magnetic resonance imaging in head and neck tumors. *Quant Imaging Med Surg*. 2018;8(10):1052-1065. [CrossRef]
10. Kamimura K, Nakajo M, Yoneyama T, et al. Assessment of microvessel perfusion of pituitary adenomas: a feasibility study using turbo spin-echo-based intravoxel incoherent motion imaging. *Eur Radiol*. 2020;30(4):1908-1917. [CrossRef]
11. Wan Q, Lei Q, Wang P, et al. Intravoxel incoherent motion diffusion-weighted imaging of lung cancer: comparison between turbo spin-echo and echo-planar imaging. *J Comput Assist Tomogr*. 2020;44(3):334-340. [CrossRef]
12. Noij DP, Martens RM, Marcus JT, et al. Intravoxel incoherent motion magnetic resonance imaging in head and neck cancer: a systematic review of the diagnostic and prognostic value. *Oral Oncol*. 2017;68:81-91. [CrossRef]
13. Dudau C, Draper A, Gkagkanasiou M, Charles-Edwards G, Pai I, Connor S. Cholesteatoma: multishot echo-planar vs non echo-planar diffusion-weighted MRI for the prediction of middle ear and mastoid cholesteatoma. *BJR Open*. 2019;1(1):20180015. [CrossRef]
14. Hirata K, Nakaura T, Okuaki T, et al. Comparison of the image quality of turbo spin echo- and echo-planar diffusion-weighted images of the oral cavity. *Medicine (Baltimore)*. 2018;97(19):e0447. [CrossRef]
15. Riffel P, Michaely HJ, Morelli JN, et al. Zoomed EPI-DWI of the head and neck with two-dimensional, spatially-selective radiofrequency excitation pulses. *Eur Radiol*. 2014;24(10):2507-2512. [CrossRef]
16. Wiesmueller M, Wuest W, May MS, et al. Comparison of readout-segmented echo-planar imaging and single-shot TSE DWI for cholesteatoma diagnostics. *AJNR*

Am J Neuroradiol. 2021;42(7):1305-1312. [CrossRef]

17. Mori N, Mugikura S, Miyashita M, et al. Turbo Spin-echo diffusion-weighted imaging compared with single-shot echo-planar diffusion-weighted imaging: image quality and diagnostic performance when differentiating between ductal carcinoma in situ and invasive ductal carcinoma. *Magn Reson Med Sci*. 2021;20(1):60-68. [CrossRef]
18. Yoshizako T, Yoshida R, Asou H, Nakamura M, Kitagaki H. Comparison between turbo spin-echo and echo planar diffusion-weighted imaging of the female pelvis with 3T MRI. *Acta Radiol Open*. 2021;10(2):2058460121994737. [CrossRef]
19. Lei Q, Wan Q, Liu L, et al. Values of apparent diffusion coefficient and lesion-to-spinal cord signal intensity in diagnosing solitary pulmonary lesions: turbo spin-echo versus echo-planar imaging diffusion-weighted imaging. *Biomed Res Int*. 2021:3345953. [CrossRef]
20. Panyarak W, Chikui T, Yamashita Y, Kamitani T, Yoshiura K. Image quality and ADC assessment in turbo spin-echo and echo-planar diffusion-weighted mr imaging of tumors of the head and neck. *Acad Radiol*. 2019;26(10):e305-e316. [CrossRef]
21. Mikayama R, Yabuuchi H, Sonoda S, et al. Comparison of intravoxel incoherent motion diffusion-weighted imaging between turbo spin-echo and echo-planar imaging of the head and neck. *Eur Radiol*. 2018;28(1):316-324. [CrossRef]
22. Baltzer PA, Renz DM, Herrmann KH, et al. Diffusion-weighted imaging (DWI) in MR mammography (MRM): clinical comparison of echo planar imaging (EPI) and half-Fourier single-shot turbo spin echo (HASTE) diffusion techniques. *Eur Radiol*. 2009;19(7):1612-1620. [CrossRef]
23. Suzuki M, Morita S, Goto Y, et al. Artifact-robust diffusion-weighted whole-body imaging with background suppression at 3 T using improved turbo spin-echo diffusion-weighted imaging. *Br J Radiol*. 2019;92(1094):20180489. [CrossRef]
24. Sakamoto J, Sasaki Y, Otonari-Yamamoto M, Nishikawa K, Sano T. Diffusion-weighted imaging of the head and neck with HASTE: influence of imaging parameters on image quality. *Oral Radiology*. 2012;28(2);87-94. [CrossRef]
25. Tyagi N, Cloutier M, Zakian K, Deasy JO, Hunt M, Rimner A. Diffusion-weighted MRI of the lung at 3T evaluated using echo-planar-based and single-shot turbo spin-echo-based acquisition techniques for radiotherapy applications. *J Appl Clin Med Phys*. 2019;20(1):284-292. [CrossRef]
26. Edelstein WA, Glover GH, Hardy CJ, Redington RW. The intrinsic signal-to-noise ratio in NMR imaging. *Magn Reson Med*. 1986;3(4):604-618. [CrossRef]
27. Heverhagen JT. Noise measurement and estimation in MR imaging experiments. *Radiology*. 2007;245(3):638-639. [CrossRef]
28. Marzi S, Piludu F, Vidiri A. Assessment of diffusion parameters by intravoxel incoherent motion MRI in head and neck squamous cell carcinoma. *NMR Biomed*. 2013;26(12):1806-1814. [CrossRef]
29. Hilbert F, Wech T, Neubauer H, Veldhoen S, Bley TA, Köstler H. Comparison of Turbo Spin Echo and Echo Planar Imaging for intravoxel incoherent motion and diffusion tensor imaging of the kidney at 3Tesla. *Z Med Phys*. 2017;27(3):193-201. [CrossRef]
30. Jiang J, Yin J, Cui L, et al. Lung Cancer: Short-Term Reproducibility of Intravoxel Incoherent Motion Parameters and Apparent Diffusion Coefficient at 3T. *J Magn Reson Imaging*. 2018;47(4):1003-1012. [CrossRef]
31. Lecler A, Savatovsky J, Balvay D, et al. Repeatability of apparent diffusion coefficient and intravoxel incoherent motion parameters at 3.0 Tesla in orbital lesions. *Eur Radiol*. 2017;27(12):5094-5103. [CrossRef]
32. Verhappen MH, Pouwels PJ, Ljumanovic R, et al. A. Diffusion-weighted MR imaging in head and neck cancer: comparison between half-fourier acquired single-shot turbo spin-echo and EPI techniques. *AJNR Am J Neuroradiol*. 2012;33(7):1239-1246. [CrossRef]